Linear-Free Energy Relationships for Modeling Structure−Reactivity Trends in Controlled Radical Polymerization

Ching Yeh Lin,[†] Sylvain R. A. Marque,[‡] Krzysztof Matyjaszewski,[§] and Michelle L. Coote[†,*]

[†]ARC Centre of Excellence for Free-Radical Chemistry and Biotechnology, Research School of Chemistry, Australian National University, Canberra ACT 0200, Australia

[‡]UMR 6264 Laboratoire Chimie Provence, case 521, Universite de Provence, Avenue Escadrille Normandie Niemen, 13397 Marseille Cedex 20, France

[§]Department of Chemistry, Carnegie Mellon University, 4400 Fifth Avenue, Pittsburgh, Pennsylvania 15213, United States

S *Supporting Information*

ABSTRACT: A set of 303 R−X bond dissociation free energies (BDFEs) at 298.15 K in acetonitrile, along with corresponding values of polar, steric and radical stability or resonance descriptors for each R-group and X-group, has been calculated at the G3(MP2)-RAD level of theory in conjunction with CPCM solvation energies. The R-groups were chosen to cover the broad spectrum of steric, polar and radical stability properties of propagating polymeric radicals, while the X-groups included a variety of nitroxides, dithioester fragments ($^{\bullet}SC(Z)=S$) and

halogens, chosen to be representative of control agents used in nitroxide mediated polymerization (NMP), reversible addition−fragmentation chain transfer (RAFT) polymerization and atom transfer radical polymerization (ATRP). The data have been used to design, parametrize and test a linear free energy relationship that can predict the BDFEs of any R and X combination based on the polar, steric and radical stability or resonance properties of the separate R and X groups. The final equation is $BDFE[R-X] = -20.8\,\theta[R] - 9.73\,IP[R] - 1.10\,RSE[R] + 192\,\theta[X] + 57.4\,EA[X] - 62.0\,Resonance[X] - 250$, where the steric descriptors $\theta[R]$ and $\theta[X]$ are measured as Tolman's cone angle of Cl−R and CH_3−X respectively, the polar descriptors $IP[R]$ and $EA[X]$ are the (gas-phase) ionization energy of $R^{\bullet}$ and electron affinity of $X^{\bullet}$ respectively, and the radical stability or resonance descriptors $RSE[R]$ and $Resonance[X]$ are measured as the standard radical stabilization energy for $R^{\bullet}$ and the inverse HOMO−LUMO energy gap for $X^{\bullet}$. This general model was also fitted to the individual cases of ATRP, RAFT, and NMP and was used to analyze similarities and differences in structure−reactivity trends among the different types of polymerization process. We show how the equation can be used to select appropriate initial leaving groups for a given polymerization, or predict the correct sequence of monomer addition in block copolymer synthesis.
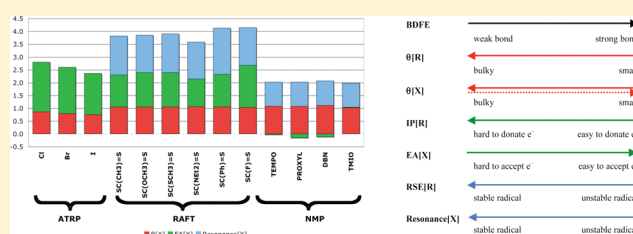
INTRODUCTION

Correlation between structure and reactivity is perhaps the most fundamental problem in chemistry; successful correlations not only aid our understanding but also allow us to predict the outcome of chemical reactions and rationally design optimal reagents. Such correlations are particularly valuable for optimizing controlled radical polymerization processes such as nitroxide mediated polymerization (NMP),[1] atom transfer radical polymerization (ATRP),[2] and reversible addition−fragmentation chain transfer (RAFT) polymerization[3] because, on the one hand, the success or failure of a process can be affected by relatively small changes to the rate and/or equilibrium constants of the control reactions; on the other hand, these rate and equilibrium constants are highly sensitive to small changes to the substitution patterns on the various reagents. In recent years there has therefore been considerable interest in using theory and/or experiment to model and explain structure−reactivity trends in NMP,[4,5] ATRP,[6] and RAFT[7] polymerization. However, the vast

majority of these studies have been largely qualitative in nature, providing at best rankings of reagent reactivities and qualitative guidelines for matching suitable control agents to particular polymerizations. For ease of use in the wider polymer chemistry community, it would be desirable to place these studies on a more quantitative footing and develop simple equations for predicting the kinetic or thermodynamic behavior for any given combination of control agent and monomer—the equivalent of a $Q−e$ scheme[8] for controlled radical polymerization.

The first step toward such a structure−reactivity correlation was presented a few years ago, when the rate constants of dissociation of various alkoxyamines were correlated with three empirical factors: Rüchardt's radical stabilization parameter as well as the Charton polar and steric parameters.[4] Excellent

correlations were derived for the case of a fixed nitroxide and variable alkyl radical; reasonable correlations were also reported for the more difficult case of a fixed alkyl radical and variable nitroxide. The utility of these equations was highlighted when they were used successfully in the design of a nitroxide capable of controlling the polymerization of methyl methacrylate.[9] Recently, we published improved versions of these equations that were capable of modeling *simultaneous* variation of the nitroxide and alkyl radical structure.[5] As part of this work we also replaced the original stability, polar and steric descriptors with new ones that are more easily accessible and extendable to larger species. We showed that the gas-phase equilibrium constants (K_{eq}) at 298.15K for the combination reaction could be well described by the equation $\log(K_{eq}) = -0.10 \text{IP} - 0.177 \text{RSE} - 0.130 \text{RSE}_{nxd} + 38.3$, where IP is the ionization potential of the alkyl radical, RSE is the radical stabilization energy of alkyl radical, and RSE_{nxd} is the radical stabilization energy of the nitroxide radical. Variants of the equation were also successfully fitted to available experimental rate coefficients for both the combination (k_c) and dissociation (k_d) reactions; however the inclusion of an additional parameter to describe the steric bulk of the alkyl group (Tolman's cone angle, θ) was found to be necessary for the fitting of k_d due to the importance of additional steric effects present in the transition state of the reaction.

With these equations in hand, we are now in a position to generalize them further so that they can model other controlled radical polymerization processes such as RAFT and ATRP, hence providing a truly general equation for selecting not only the optimal control agent for a given monomer, but also the optimal type of controlled radical polymerization process. In order to model the simultaneous variation of the control agent and alkyl group across several different types of controlled radical polymerization processes, we need to study their thermodynamics in the same type of chemical reaction. To this end, in the present work we model substituent effects on the R–X bond dissociation free energy (BDFE) in acetonitrile solution, where R• is the propagation polymeric or initiating radical, and X• is either the halogen atom in ATRP, the nitroxide radical in NMP, or a RAFT agent fragment of the form •SC(Z)=S. Prima facie, this choice of reaction might seem unusual. Whereas the controlling reaction in NMP is the R–X homolysis reaction, for ATRP and RAFT this reaction does not occur during the process itself and the X• or •SC(Z)=S radicals are not actually formed as intermediates. Thus, for example, in ATRP the real equilibrium constant of relevance depends on the difference of the R–X BDFE and the Cu–X BDFE of the catalyst; in RAFT the real equilibrium constant of relevance is not a homolysis reaction but rather a radical addition of R• to the C=S bond of the RAFT agent. However, as seen from Scheme 1, the chain transfer processes that do occur in these latter processes can be represented as the *difference* of two such R–X BDFEs. In this way, equations for predicting R–X BDFEs can be used to choose optimal initiators (or leaving groups in RAFT) or identify the correct comonomer addition sequence to form well-defined block copolymers. It is true that the resulting equations are not suitable for optimizing the kinetics of the exchange rate between the dormant and active species, particularly in the case of RAFT polymerization where this is dominated by the radical addition to the thiocarbonyl double bond and the β-scission of the resulting intermediate. However, based on our success with modeling the kinetics of NMP,[4,5] we expect that the polar, steric and radical stability or resonance

Scheme 1. Relationship between R−X BDFEs and Chain Transfer Processes in ATRP, NMP, and RAFT
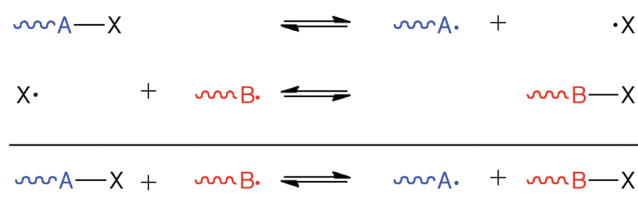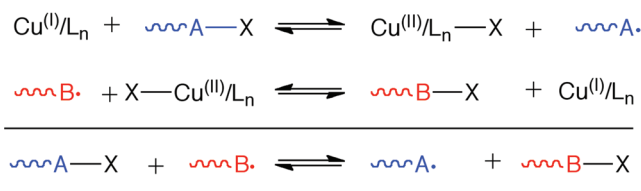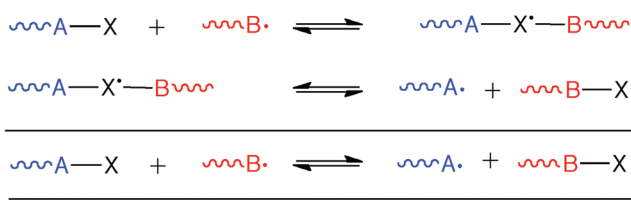

descriptors developed in the present work will remain useful when developing linear free energy relationships for these kinetic factors.

In what follows, we use high-level ab initio molecular orbital theory calculations to obtain values of the R−X BDFEs for the various combinations of the R-groups and X-groups relevant to NMP, ATRP, and RAFT, as well as values of a variety of polar, steric and radical stability or resonance descriptors of the various X• and R• groups. Using these values we design, fit, and test various linear free energy relationships for predicting R−X BDFEs as a function of the isolated properties of R• and X•, with a view to identifying a general equation capable of modeling substituent effects across these various controlled radical polymerization processes. We then show how these equations may be used in practice to determine optimal leaving groups or monomer addition sequences in block copolymer synthesis.

■ COMPUTATIONAL PROCEDURES

High-level ab initio molecular orbital theory calculations, performed using Gaussian 03[10] and Molpro 2009.1,[11] were used to calculate the R−X BDFEs, as well as values of the various polar, steric and radical stability or resonance descriptors for R• and X•. Calculations were performed at a high level of theory, chosen on the basis of previous assessment studies for radical stabilization energies and associated bond dissociation energies,[12] as well as the equilibrium constants in ATRP,[6c,13] NMP,[5,14] and RAFT,[15] and the ionization energies, electron affinities and associated solution-phase redox potentials of alkyl radicals,[13] alkyl halides[13] and nitroxide radicals.[16] Geometries were optimized at the

Table 1. Bond Dissociation Free Energies (BDFEs, kJ/mol) in acetonitrile at 298.15K for the Training Set[a]

R[b]	Cl	Br	SC(CH₃)=S	TEMPO
iPPh	286.3	224.8	163.3	87.8
VPh	281.5	222.8	183.5	98.6
MPh	283.9	228.0	190.9	109.9
iPCOOMe	280.4	220.5	179.2	98.1
VCOOMe	288.8	231.6	195.1	116.5
MCOOMe	297.6	241.9	211.7	133.0
iPCN	269.5	209.5	164.9	94.3
VCN	269.7	212.2	178.2	111.2
MCN	280.6	225.8	193.8	124.7
VCH=CH₂	268.9	210.9	166.1	81.4
MCH=CH₂	274.7	218.6	179.3	100.4
cHdene	241.6	185.6	143.0	52.8
MC≡CMe	274.4	218.7	187.2	108.8
VCOEt	287.9	229.8	186.3	111.5
nHex	331.9	274.4	235.5	158.8
cHex	336.7	277.3	234.0	150.4
tBu	334.3	272.5	216.1	131.8
PCOOH	286.9	229.6	189.4	93.4
iPCOOH	278.0	217.9	176.6	82.3
VCOOH	287.3	230.1	194.8	114.9
Me	334.8	279.1	247.2	160.7

[a] Calculations performed at the G3(MP2)-RAD//B3-LYP/6-31G(d) level of theory in conjunction with CPCM-UAHF solvation energies (see text for further details). [b] Chemical structures provided in Scheme 2.

Table 2. Bond Dissociation Free Energies (BDFEs, kJ/mol) in acetonitrile at 298.15K for Test Set I[a]

R[b]	Cl	Br	SC(CH₃)=S	TEMPO
Et	330.0	272.1	235.2	159.0
P	329.3	271.6	233.2	158.9
iP	331.6	271.7	227.9	145.3
MCOOH	302.7	246.2	210.4	128.6
MCOOEt	297.9	242.2	205.5	129.0
VCOOEt	289.1	231.8	193.8	116.5
iPCOOEt	282.4	222.4	165.4	98.6
VCOOtBu	291.1	233.7	194.1	113.4
MC≡CH	275.3	219.8	185.9	110.2
VCOMe	288.7	230.6	182.9	100.3
MCONH₂	305.9	247.3	213.0	138.8
VCONH₂	293.7	233.6	200.5	124.7
iPCONH₂	296.2	232.1	174.4	99.2
VCONMe₂	295.8	238.2	199.5	116.4
VCONEt₂	293.9	236.2	200.4	116.6
VOMe	330.8	269.9	213.0	159.1
MOCOMe	321.1	260.3	222.5	170.2
VOCOMe	321.8	259.4	215.3	165.3
iPOCOMe	320.5	256.4	194.3	151.7
MOH	328.5	267.4	223.9	168.5
MF	330.8	267.4	229.7	194.7
MCl	307.5	248.0	215.2	149.3
VF	331.7	267.2	223.9	193.5
VCl	308.5	247.1	211.5	156.7
VBr	308.8	247.7	214.4	155.5
iPCl	308.2	246.6	196.9	141.4
PCl	306.2	245.0	207.3	152.6
VF₂	333.6	265.1	208.0	204.3
VCl₂	287.6	224.3	180.8	141.8
MCl₂	291.0	229.5	198.0	158.6
MCl₃	268.7	206.4	171.2	137.0
V(Ph)COOMe	253.9	192.6	158.6	82.2
V(Ph)₂	258.6	199.0	161.2	84.4
V(COOMe)₂	283.6	226.4	191.2	118.1
iP(COOMe)₂	278.3	218.2	178.3	99.6
iPCH=CH₂	268.0	207.8	149.6	64.2
VC(CH₃)=CH₂	275.0	215.9	174.6	90.6
MC(CH₃)=CHCH₃	274.7	218.6	180.2	98.6
MCH=C(CH₃)₂	268.5	213.4	174.8	93.2

[a] Calculations performed at the G3(MP2)-RAD//B3-LYP/6-31G(d) level of theory in conjunction with CPCM-UAHF solvation energies (see text for further details). [b] Chemical structures provided in Scheme 2.

B3LYP/6-31G(d) level of theory, and frequencies were also calculated at this level and scaled by the recommended[17] scale factors. Our energy-directed tree search method[18] was used for conformational searching.

Improved energies were calculated at the G3(MP2)-RAD level of theory, a high-level composite ab initio molecular orbital theory method that approximates CCSD(T) calculations with a large triple-ζ basis from calculations with a double-ζ basis set, via basis corrections carried out the R(O)MP2 level of theory.[19] Where full G3(MP2)-RAD calculations were impractical, an ONIOM approximation was used in which the core (designed to include the reaction center, all alpha substituents and any other substituents conjugated with it) was studied at G3(MP2)-RAD, and the remaining remote substituent effects were modeled at R-(O)MP2/G3MP2Large.[20] For species containing third-row atoms, we adopted Rassolov's 6-31G[21] rather than the default basis sets in Gaussian. Rassolov's 6-31G basis set is consistent with first- and second-row atoms, whereas the default Gaussian 6-31G basis set is not. For species containing fourth-row atoms, all calculations with the 6-31G(d) basis set were performed with the effective core potential LACVP*; calculations with the G3MP2Large basis set were performed using the all-electron basis 6-311+G(3df,2p). The ionization potentials (IPs) are computed from gas phase G3(MP2)-RAD energies including zero point energy at 0K and electron affinities (EAs) are computed from gas phase G3(MP2)-RAD(+) energies including zero point energy at 0K where (+) denotes inclusion of an extra diffuse function on the small basis set calculations (i.e., 6-31+G(d) were used instead of 6-31G(d) or LACVP+* were used instead of LACVP*) to compensate the weakly bounded electron of the anion. The lowest unoccupied molecular orbital (LUMO) and highest occupied molecular orbital (HOMO) energies that are used to calculate the resonance parameter are taken from the UHF/STO-3G//B3LYP/6-31G(d) calculations in order to avoid interference from Rydberg states that are often introduced in larger basis set

calculations. Because, for reasons of accuracy, we use unrestricted wave functions for these calculations, we consistently use the energies of relevant α spin orbitals when calculating the various *molecular orbital* energy gaps (i.e., the HOMO−LUMO gap is the α-HOMO to α-LUMO gap).

Having obtained the geometries, frequencies and improved energies, gas-phase enthalpies, entropies and free-energies at 298.15 K were obtained using the standard textbook formulas for the statistical thermodynamics of an ideal gas under harmonic oscillator/rigid rotor approximation, as implemented using our in-house *T-Chem* program.[22] Solvation energies in acetonitrile were calculated using the popular continuum model CPCM[23] in conjunction with the UAHF radii.

Table 3. Bond Dissociation Free Energies (BDFEs, kJ/mol) in acetonitrile at 298.15K for Test Set II[a]

R[b]	I	SC(OCH₃)=S	SC(SCH₃)=S	SC(NEt₂)=S	SC(Ph)=S	SC(F)=S	PROXYL	DBN	TMIO
VOCOMe (VA)	203.1	210.8	213.1	196.7	208.1	228.4	156.8	159.5	162.1
VCOOMe (MA)	183.8	196.3	196.7	176.0	188.5	207.5	108.4	108.0	111.1
iPCOOMe (MMA)	171.1	176.7	179.8	159.5	173.9	195.0	91.2	90.8	94.4
VPh (STY)	172.8	179.9	183.6	162.6	177.4	199.5	91.4	87.4	97.2
VCOOH (AA)	182.1	189.8	193.4	175.4	187.7	205.2	108.3	106.0	108.5
VCONH₂ (AM)	189.0	194.6	198.0	182.0	192.1	219.9	117.5	112.4	119.6
VCN (AN)	164.1	174.3	180.4	162.2	171.7	191.5	99.8	103.1	105.0

[a] Calculations performed at the G3(MP2)-RAD//B3-LYP/6-31G(d) level of theory in conjunction with CPCM-UAHF solvation energies (see text for further details). [b] Chemical structures provided in Scheme 2.

Scheme 2. Data Sets in the Present Study
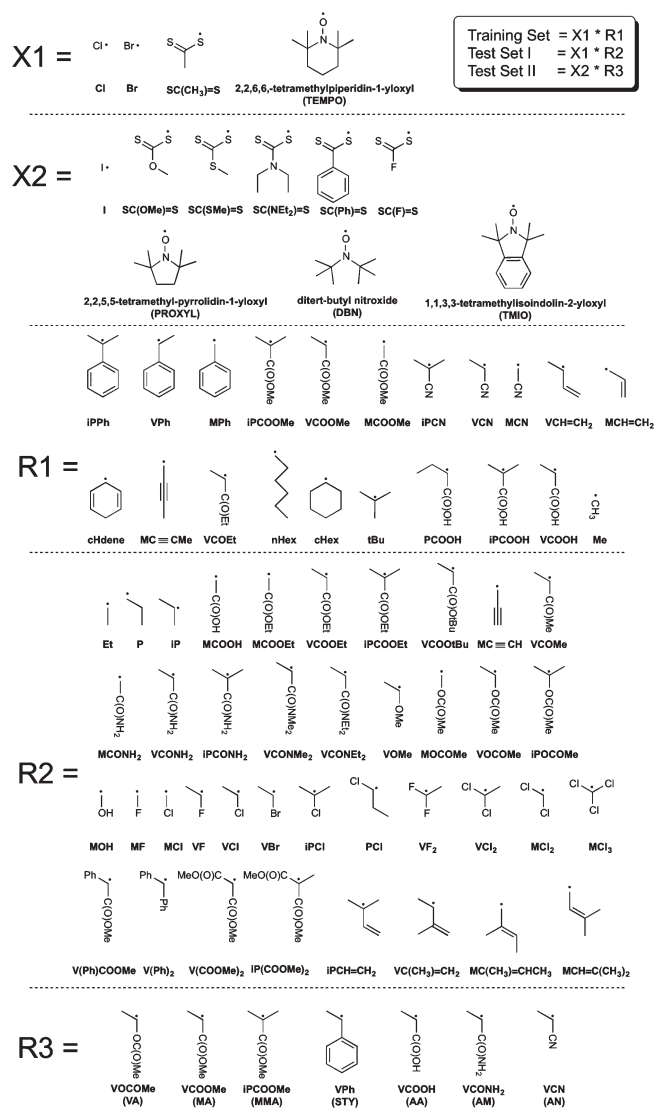
Geometries were reoptimized in the solvent field using UHF/6-31 +G(d) and solvation energies were obtained from ROHF/6-31+G(d). Free energies of each species in solution were then obtained as the sum of the corresponding gas-phase free energy, the calculated free energy of solvation and a correction term, $RT \ln(24.46)$, to take account of the fact that the solvation energy is computed for the passage from 1 atm (g) to 1 mol L^{-1} (soln).

RESULTS AND DISCUSSION

Data. Tables 1−3 show the R−X BDFEs at 298.15 K in acetonitrile for the various combinations of the R-groups and X-groups in Scheme 2; corresponding gas-phase data are provided in Table S1 of the Supporting Information. Values of a variety of polar, steric and radical stability or resonance descriptors for the R$^\bullet$ and X$^\bullet$ groups were also calculated and are provided in Tables 4 and 5, respectively. As seen in Scheme 2, we divided our data into a training set of representative R-groups reacting with X groups representative of ATRP (Cl, Br), NMP (2,2,6,6,-tetramethylpiperidin-1-yloxyl, TEMPO) and RAFT (SC(CH₃)=S), and two test sets: Test set I includes an expanded range of R-groups; test set II contains an expanded range of X-groups. Models were initially fitted to the training set, their predictions were then tested on the relevant test set(s) and then the final models were obtained by refitting to all available data. Throughout this work, all model fitting is based on the solution phase BDFEs; corresponding equations for the gas-phase BDFEs are qualitatively similar and are provided in the Supporting Information (see Table S2 and S3).

Effect of R for Fixed X. As in our previous study of NMP,[5] we initially examined the effect of R on the BDFE while keeping X fixed. Separate fitted equations were then obtained and compared for each studied X value. Using the training set, we first fitted the equations of the form,

$$BDFE[R-X] = a\upsilon[R] + b\sigma_U[R] + c\sigma_{RS}[R] + d \quad (1)$$

$$BDFE[R-X] = a\theta[R] + bIP[R] + cRSE[R] + d \quad (2)$$

Here all descriptors refer to the R-group, and υ and σ_U are the Charton steric and polar parameters, σ_{RS} is the Rüchardt radical stability parameter, θ is the Tolman's cone angle (in radian) as defined in ref 5 IP is the gas-phase ionization potential at 0K (in eV) and RSE is the standard radical stabilization energy (in kJ mol^{-1}) at 298.15K. Further information on how the various R$^\bullet$ descriptors are defined and calculated is available in our previous study of NMP, where we also explain the basis for choosing our new descriptors (RSE, IP, θ) over alternatives (e.g., the use of IP instead of electron affinity EA or dipole moment μ).[5] The first equation is analogous to the original linear free energy relationship for NMP.[4] The second equation is analogous to our recently updated equation except that it includes a steric parameter (θ), which in our previous study of NMP was only required for modeling the decomposition kinetics.[5] Table 6 shows the resulting fitted parameters for each model, along with the R^2 value and mean absolute deviation (MAD) of the fitted values

Table 4. Descriptors of R[•] Used in the Linear Free Energy Relationships: Normalized Values of the Rüchardt RSE (σ_{RS}); the standard Radical Stabililization Energy (RSE, kJ/mol); the Charton Steric Parameter (υ); Tolman's Cone Angle (θ, rad); the Charton Parameter for Polar/Inductive Field (σ_U); the Ionization Potential (IP, eV)[a]

R group	radical stability		steric		polar	
	σ_{RS}	RSE	υ	θ	σ_U	IP
iPPh	0.36	69.72	1.28	2.67	0.05	6.73
VPh	0.34	68.27	0.86	2.37	0.07	7.03
MPh	0.31	61.03	0.70	2.06	0.03	7.39
iPCOOMe	0.20	54.65	1.43	2.58	0.07	8.27
VCOOMe	0.18	41.96	1.00	2.34	0.09	8.92
MCOOMe	0.15	23.24	0.80	2.13	0.15	9.91
iPCN	0.22	58.38	1.20	2.46	0.14	8.64
VCN	0.19	45.93	0.79	2.25	0.17	9.36
MCN	0.16	32.52	0.58	2.04	0.20	10.31
VCH=CH$_2$	0.46	84.60	0.86	2.27	0.03	7.66
MCH=CH$_2$	0.43	72.02	0.69	2.04	0.02	8.27
cHdene	0.54	116.20	0.72[b]	2.24	0.07	6.95
MC≡CMe	0.25	51.40	0.72	2.08	0.12	8.02
VCOEt	0.28	43.38	0.82	2.56	0.09	8.87
nHex	0.07	10.28	0.73	2.05	−0.01	8.25
cHex	0.10	20.19	0.87	2.25	0.00	7.54
tBu	0.12	28.55	1.24	2.47	−0.01	7.22
PCOOH	0.18	39.73	1.02	2.55	0.09	9.09
iPCOOH	0.21	55.77	1.24	2.55	0.07	8.54
VCOOH	0.18	41.89	0.83	2.29	0.09	9.24
Me	0.00	0	0.52	1.85	−0.01	9.88
Et	-	13.54	-	2.05	-	8.63
P	-	10.09	-	2.04	-	8.49
iP	-	23.06	-	2.26	-	7.80
MCOOH	-	22.72	-	2.21	-	10.32
MCOOEt	-	23.43	-	2.28	-	9.79
VCOOEt	-	42.04	-	2.34	-	8.83
iPCOOEt	-	54.78	-	2.58	-	8.19
VCOOtBu	-	41.85	-	2.56	-	8.67
MC≡CH	-	52.87	-	2.03	-	8.76
VCOMe	-	50.79	-	2.49	-	9.06
MCONH$_2$	-	23.44	-	2.39	-	9.77
VCONH$_2$	-	42.18	-	2.60	-	8.79
iPCONH$_2$	-	50.89	-	2.84	-	8.18
VCONMe$_2$	-	38.62	-	2.57	-	8.26
VCONEt$_2$	-	40.16	-	2.51	-	8.09
VOMe	-	36.50	-	2.48	-	7.16
MOCOMe	-	18.43	-	2.11	-	8.29
VOCOMe	-	24.37	-	2.33	-	7.65
iPOCOMe	-	17.60	-	2.67	-	7.45
MOH	-	32.32	-	1.98	-	8.21
MF	-	12.81	-	1.98	-	9.61
MCl	-	20.30	-	2.05	-	8.94
VF	-	19.70	-	2.18	-	8.64
VCl	-	26.72	-	2.26	-	8.27
VBr	-	23.15	-	2.28	-	8.21
iPCl	-	30.69	-	2.48	-	7.75

Table 4. Continued

R group	radical stability		steric		polar	
	σ_{RS}	RSE	υ	θ	σ_U	IP
PCl	-	25.98	-	2.53	-	8.13
VF$_2$	-	10.65	-	2.31	-	9.30
VCl$_2$	-	35.45	-	2.49	-	8.26
MCl$_2$	-	32.27	-	2.27	-	8.75
MCl$_3$	-	42.57	-	2.51	-	8.73
V(Ph)COOMe	-	80.30	-	2.45	-	7.72
V(Ph)$_2$	-	85.64	-	2.59	-	6.72
V(COOMe)$_2$	-	29.13	-	2.52	-	9.89
iP(COOMe)$_2$	-	43.62	-	2.76	-	9.04
iPCH=CH$_2$	-	89.97	-	2.47	-	7.29
VC(CH$_3$)=CH$_2$	-	76.72	-	2.50	-	7.43
MC(CH$_3$)=CHCH$_3$	-	70.99	-	2.29	-	7.43
MCH=C(CH$_3$)$_2$	-	77.28	-	2.04	-	7.29
VOCOMe (VA)	-	24.37	-	2.33	-	7.65
VCOOMe (MA)	0.18	41.96	1.00	2.34	0.09	8.92
iPCOOMe (MMA)	0.20	54.65	1.43	2.58	0.07	8.27
VPh (STY)	0.34	68.27	0.86	2.37	0.07	7.03
VCOOH (AA)	0.18	41.89	0.83	2.29	0.09	9.24
VCONH$_2$ (AM)	-	42.18	-	2.60	-	8.79
VCN (AN)	0.19	45.93	0.79	2.25	0.17	9.36

[a] Full description of each of the descriptors can be found in ref 5. The Charton and Rüchardt descriptors are empirical values that are taken directly from ref 4b or references cited therein. The RSE values are calculated as ΔH_{gas} at 298 K using G3(MP2)-RAD for the reaction R[•] + CH$_4$ → R−H + [•]CH$_3$. θ are computed from B3LYP/6-31G(d) optimized R-Cl geometries. IP are computed from gas phase G3-(MP2)-RAD energy for R[•] → R[+] + e[−] including zero point energy at 0 K. [b] For this alkyl group, the steric descriptor was estimated in the reference above. It was described that this value for steric parameter should be sterically *more* demanding than cyclohexane ($u = 0.87$) but *less* than the phenyl group ($u = 2.15$), however, the steric descriptor of phenyl ring is 0.57 from the original Charton's paper, and intuitively should be steric *less* demanding than cyclohexane but *more* than the phenyl ring, here, we corrected this value from 1.5 to (0.87 + 0.57)/2 = 0.72.

from the actual values. It should be stressed that, unlike the subsequent more general models, this statistical testing is performed on the same restricted data set to which each individual equation is fitted.

From Table 6, we first note that both models can be successfully fitted to each individual set of BDFEs for each type of controlled radical polymerization process. The MADs for eq 2 are marginally lower than for eq 1, but both provide a reasonable description of structure−reactivity trends in the chain transfer energies within each type of polymerization process. However, as noted in our previous study, a disadvantage of eq 1 is that values of the semiempirical descriptors (υ, σ_U, and σ_{RS}) are not readily available in the literature (and not easy to measure) for many of the required substituents including those in our test sets. By contrast the R-descriptors of eq 2 are easy to obtain via theory or experiment, even for larger and more unusual substituents. For this reason, we adopt these latter R-descriptors (i.e., θ, IP, and RSE) for the present work.

As noted previously,[5] we can use the fitted coefficients of the steric, polar, and radical stability terms (a, b and c) to calculate

Table 5. Resonance (1/LUMO−HOMO gap, 1/Hartree), Steric (Tolman's Cone Angle θ, rad) and Polar (Electron Affinity, EA, eV) Descriptors of $X^{\bullet}$ [a]

	X	resonance	steric θ	polar EA
halogens (ATRP)	Cl	0	2.64	3.69
	Br	0	2.45	3.42
	I	0	2.32	3.05
dithioesters (RAFT)	SC(CH$_3$)=S	2.20	3.23	2.37
	SC(OCH$_3$)=S	2.11	3.23	2.54
	SC(SCH$_3$)=S	2.18	3.23	2.55
	SC(NEt$_2$)=S	2.08	3.28	2.05
	SC(Ph)=S	2.61	3.25	2.40
	SC(F)=S	2.13	3.19	3.11
nitroxides (NMP)	TEMPO	1.36	3.34	−0.05
	PROXYL	1.37	3.32	−0.29
	DBN	1.39	3.42	−0.22
	TMIO	1.37[b]	3.16	0.03

[a] The LUMO−HOMO gaps used to calculate the resonance descriptor are calculated at the UHF/STO-3G//B3LYP/6-31G(d) level of theory, and θ values are computed from B3LYP/6-31G(d) optimized R−Cl geometries. Values for atoms are set to zero as these do not have attached functional groups with which to undergo resonance. EA are computed from the gas phase G3(MP2)-RAD(+) energies including zero point energy at 0 K. Because we are using them as a guide to their ability to stabilize the polar configurations of a bond, rather then be reduced, we have calculated vertical values rather than adiabatic ones. [b] For TMIO the resonance descriptor is calculated from the HOMO to LUMO+3 gap, as this latter orbital matches N−C σ^* bond; the HOMO−LUMO gap gives a value of 1.97 but corresponds to the interaction of the unpaired electron and the nonconjugated π^* orbital of the aromatic ring (see text and Figure S1 of the Supporting Information for further explanation).

their relative contribution in each fitted equation via eqs 3 and 4 below (see Table 6).[24]

$$\alpha_D = \sqrt{\frac{\sum\limits_{i=1}^{n}(D_i - \bar{D})^2}{\nu}} \tag{3}$$

$$\%D = 100 \times \frac{\alpha_D C_D}{\sum\limits_{j} \alpha_{Dj} C_{Dj}} \tag{4}$$

In these equations, D_i is the value of the descriptor D for the ith data; $\bar{D}$ is the mean of the D descriptor in n number of data points; ν is the degree of freedom (which is equal to $n - 2$, where n is the number of data points); and α_D is the weighting coefficient with C_D the coefficient of the D descriptor. As expected, the % contributions of the various R-group descriptors vary according to the nature of X, with polar effects ($\sigma_U[R]$ and IP[R]) being more important for X = halogen (i.e., ATRP) and steric effects ($\upsilon[R]$ and $\theta[R]$) being greater for the nitroxides (NMP) and dithioesters (RAFT). It should be noted that the steric terms ($\upsilon[R]$ and $\theta[R]$) are not statistically significant at the 95% level of confidence for all of the ATRP cases, which is to be expected because both Cl and Br are relatively small compared with the functional groups associated with RAFT and NMP agents. The greater importance of polar effects for ATRP compared with the other processes is due to the ability of the

Table 6. Equations for Predicting R−X BDFEs in Solution as a Function of the Properties of R with Fixed X [a]

	Cl	Br	SC(CH$_3$)=S	TEMPO
BDFE[R − X] = $a\upsilon$[R] + $b\sigma_U$[R] + $c\sigma_{RS}$[R] + d				(1)
% contribution υ[R]	6[b]	10[b]	20	25
% contribution σ_U[R]	40	37	24	17
% contribution σ_{RS}[R]	54	53	56	58
a	−7.92	−14.8	−29.8	−38.3
b	−229	−221	−151	−111
c	−142	−141	−156	−165
d	346	294	258	192
R^2	0.89	0.90	0.92	0.88
MAD (kJ/mol)	7.0	6.5	8.2	6.9
BDFE[R − X] = $a\theta$[R] + bIP[R] + cRSE[R] + d				(2)
% contribution θ[R]	4[b]	7[b]	17	17
% contribution IP[R]	32	30	21	21
% contribution RSE[R]	64	63	62	62
a	−7.11	−13.8	−32.0	−34.8
b	−14.1	−13.1	−8.41	−6.54
c	−1.10	−1.07	−1.01	−1.00
d	477	425	384	294
R^2	0.93	0.93	0.95	0.96
MAD (kJ/mol)	4.8	4.9	4.7	3.8

[a] Parameters associated statistical measures obtained by fitting each equation to the relevant subset of the training set of solution-phase BDFEs in which R was allowed to vary and X was held constant. The % contributions were calculated via eqs 3 and 4. [b] These descriptors are not statistically significant at 95% level of confidence.
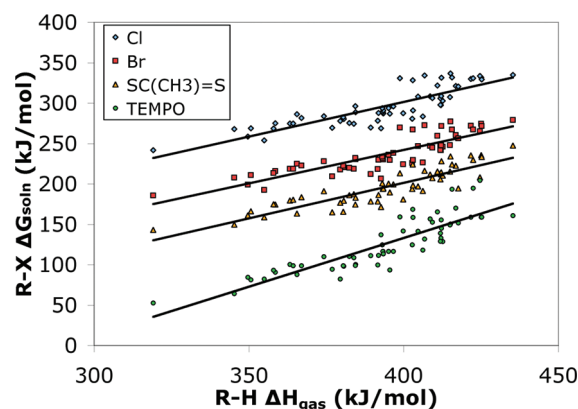
Figure 1. Correlation between R−X BDFE in acetonitrile solution (ΔG_{soln}) and R−H BDE (ΔH_{gas}). R^2 values for Cl, Br, SC(CH$_3$)=S, and TEMPO are 0.72, 0.73, 0.79, and 0.76 respectively.

halogens to undergo charge-shift bonding with electron donating alkyl groups.[25]

While there are differences in the relative importance of polar and steric effects, it is also clear from Table 6 that the radical stability descriptors (σ_{RS}[R] and RSE[R]) provide the major contribution to all BDFEs. This is further demonstrated in Figure 1, which shows a strong correlation between the R−X BDFE and the corresponding R−H bond dissociation enthalpies (BDEs). The RSEs of alkyl radicals are in fact measured as the
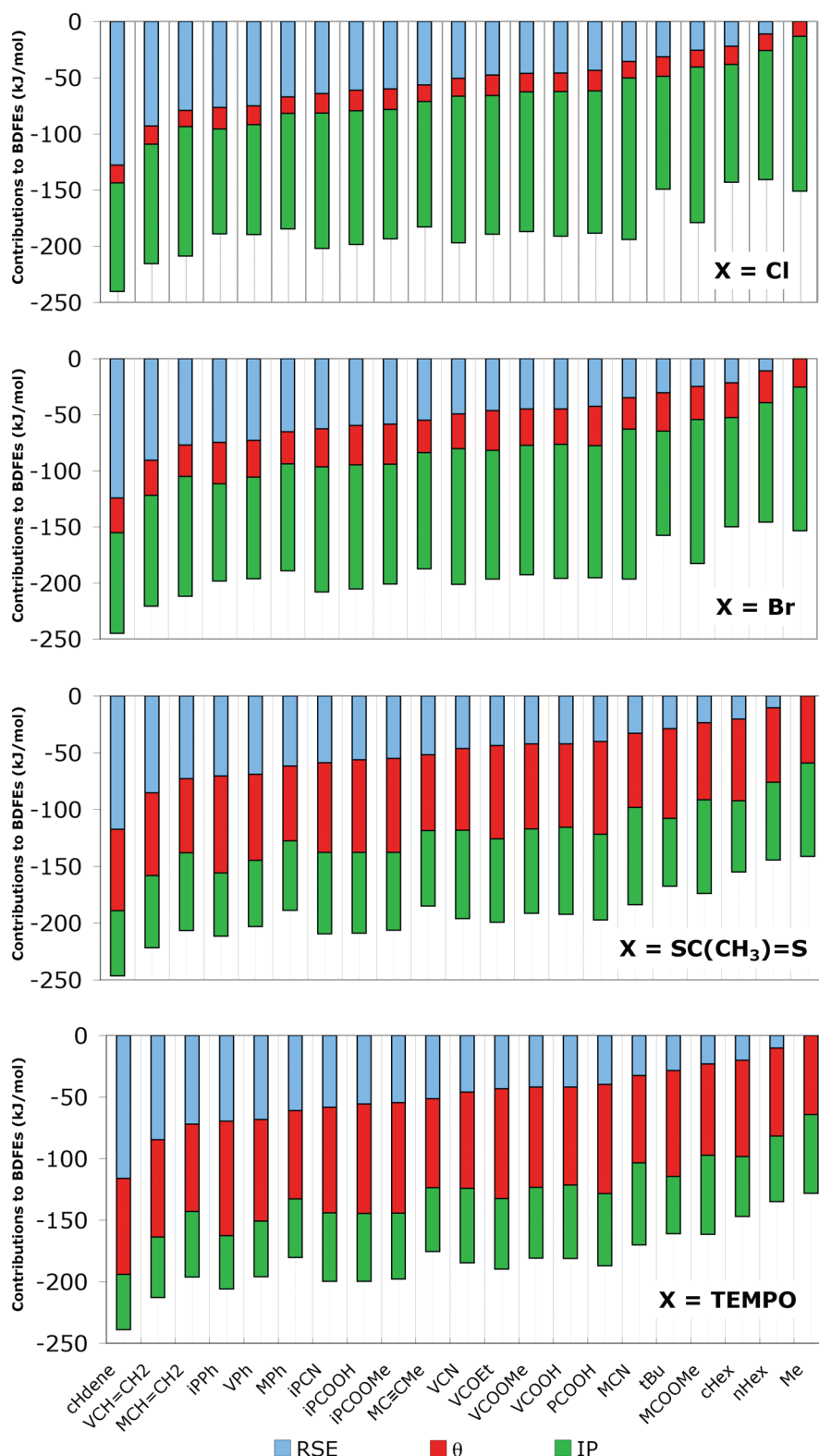
Figure 2. Steric, polar and radical stability contributions of each R-group to the various R—X BDFEs in the training set, as calculated by eq 2.

relative values of these R—H BDEs, while σ_{RS} are based on corrected values of R-CH$_3$ BDEs, and are known to be correlated with RSEs.[12] Both the RSE and σ_{RS} values are well-known to provide a good measure of the relative stability of the unpaired

electron in R$^{\bullet}$, as this is much more sensitive to substitution changes than the stability of the corresponding R—H or R—CH$_3$ bond.[12] Our present results suggest that this is also largely true of the studied R—X bonds, though polar and/or steric effects on

bond strength do also play a role and are responsible for the scatter in Figure 1.

To analyze this "scatter" further, Figure 2 shows the separate steric, polar and radical stability contributions of each R-group to the BDFEs for each X-group, as calculated by their respective version of eq 2. In each case, these contributions serve to lower the BDFEs below the respective values of the intercept term in eq 2, and hence the less negative the contribution, the stronger the bond. In other words, as expected, the BDFE increases (i.e., the bond strengthens) as the radical stability of $R^\bullet$ decreases, as its steric bulk decreases, and as its IP decreases (and hence the stability of R^+ increases). The intercept term in eq 2, which has values of 476, 423, 383, and 293 kJ mol^{-1} for X = Cl, Br, SC(CH$_3$)=S and TEMPO, respectively, is correlated with the average of the set of BDFEs to which the equation was fitted and can be loosely thought of as the inherent bonding energy in the presence of "baseline" polar, steric or radical stability effects. The BDFE contributions are ordered according to the decreasing radical stability of $R^\bullet$, with stable radicals such as those with allylic double bonds and aromatic rings at the extreme left-hand side and primary aliphatic radicals at the extreme right-hand side. These substituent effects on $R^\bullet$ radical stability have been discussed in detail elsewhere, and will not be reiterated here.[12,26] Instead, we are interested here in how these $R^\bullet$ contributions interplay with the steric and polar contributions to determine the overall BDFE.

As anticipated, there is a broad qualitative ordering of BDFE with $R^\bullet$ radical stability, but there is also some scatter due to the impact of the polar and steric contributions. These polar contributions are most pronounced for ATRP; the steric contributions are more pronounced for NMP and RAFT. For example, if we examine the series $^\bullet$C(CH$_3$)$_2$Ph (iPPh), $^\bullet$CH(CH$_3$)Ph (VPh), and $^\bullet$CH$_2$Ph (MPh), radical stability decreases from iPPh through to MPh due to decreasing hyperconjugation, and this contributes to an increase in the BDFE in this direction. At the same time, the steric bulk also decreases from iPPh through to MPh, reinforcing the increase in the BDFE in this direction. However, the decreasing opportunity for hyperconjugative interactions from iPPh through to MPh also leads to a decrease in the stability of R^+ (and hence to an increase in the IP), which would weaken the bond. For ATRP, where polar effects are dominant, this counteracts the radical stability and steric effects and leads to a fairly constant BDFE from iPPh through to MPh; for RAFT and NMP, where the polar effects are less pronounced and the steric effects more pronounced, the BDFEs increase significantly from iPPh through to MPh in accordance with trends in $R^\bullet$ radical stability.

To take one further example, the propagating radical in acrylonitrile polymerization (modeled here as VCN) has a lower radical stability and a lower steric bulk than the propagating radical in methyl methacrylate polymerization (modeled here as iPCOOMe), but has a higher IP as the CN substituent is a stronger electron withdrawing group than COOMe, and because iPCOOMe also has an additional CH$_3$ group that can stabilize R^+. As a result, according to the predictions of eq 2, the BDFE for VCN is higher than for iPCOOMe for NMP and RAFT, whereas for ATRP these BDFEs are approximately equal. In fact in the actual calculated BDFEs, as opposed to those predicted by eq 2, these polar effects in ATRP (and to a lesser extent in RAFT) are even further pronounced to the extent that the BDFE for VCN is approximately 10 kJ mol^{-1} lower than for iPCOOMe for ATRP, it is 13 kJ mol^{-1} higher for NMP and the two BDFEs

approximately equal for RAFT. This underestimation of the polar effect difference for VCN and iPCOOMe is likely due to the fact that the IP of VCN is particularly influenced by σ effects as well as π-effects on the stabilities of R^+ relative to $R^\bullet$, whereas the π-effects are much more important in determining bond strength in these examples. Across the broad set of R-groups examined, this balance between σ and π effects changes, and this in turn contributes to the underlying error of approximately ± 5 kJ mol^{-1} in the model predictions. Nonetheless, the model is able to capture and help explain the key result that electron-withdrawing monomers such as acrylonitrile tend to be proportionately less reactive (i.e., have stronger R—X bonds) in ATRP, and to a lesser extent RAFT, than in NMP; conversely, the inclusion of electron donating groups in a monomer will increase its reactivity in ATRP (and to a lesser extent RAFT) compared with NMP.

New X-Descriptors. In the previous section, we saw that the contribution of each R-descriptor has a different weighting according to the nature of X, reflecting the differing importance of polar, steric and resonance effects in each case. Since these R-descriptors are required to have the *same* weightings when developing a single equation for modeling the simultaneous variation of R and X, this implies that the X-descriptors will need to discriminate these differences in polar, steric and resonance effects. In our previous study of NMP, we used a single X-descriptor, RSE$_{nxd}$, which we defined as the relative value of the X—H BDE and a reference tBu$_2$NO-H BDE.[5] This is effectively the same as a standard RSE value, but with the values systematically shifted so that a typical nitroxide radical, tBu$_2$NO$^\bullet$, rather than CH$_3^\bullet$ is used as the zero for the scale. As we showed previously, due to the particular chemical structure of nitroxide functionality, this single descriptor captures the key resonance *and steric* contributions of X to R—X bond strength in this case. This single X-descriptor is sufficient because, within a series of nitroxides, the bonded atoms are identical at the α, β, and γ positions, and hence, many of the normal contributions to the bond energies are relatively constant. However, in the present work, we now consider the variation of X across a much broader range of X groups, where the nature of the bonded atoms can change significantly. As a result, this descriptor is likely to reflect a complex and varying interplay of the changes to covalent bond strength in X—H due to orbital overlap as well as the steric, polar, and resonance properties of X. Hence, this all-purpose parameter is unlikely to provide a useful steric, polar, or resonance descriptor for X in a general model for controlled radical polymerization.

To model the simultaneous variation of R and X we have therefore adopted three new X-descriptors. To model the steric contribution, we use Tolman's cone angle (θ) which, as outlined in ref 5 provides a direct measure of the steric crowding around the reaction center; more details on how to obtain this for X can be found in Table S4 of the Supporting Information. To model polar effects we use the gas-phase electron affinity of X$^\bullet$ (EA) at 0 K which, together with the IP of R$^\bullet$, provides a measure of the relative stability of the most stable polar configuration (R$^+$X$^-$) of the R—X bond. To model the resonance effect, we introduce a new resonance descriptor calculated as the inverse HOMO–LUMO energy gap of X$^\bullet$ (where HOMO stands for the highest occupied molecular orbital and LUMO stands for the lowest unoccupied molecular orbital). The smaller the HOMO–LUMO gap, the more easily the unpaired electron is excited into the LUMO of an adjacent substituent, and hence the stronger the
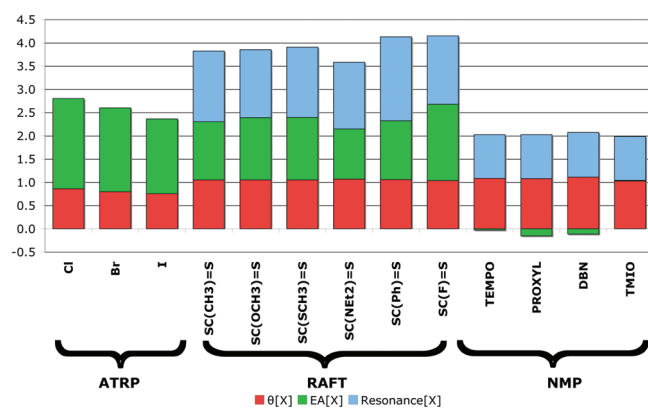
Figure 3. Values of each of the X-descriptors in dimensionless units (obtained by dividing each value by the average value for that descriptor across the full data set).

resulting conjugation (or hyperconjugation). In applying this descriptor, care is needed to make sure that the HOMO contains the unpaired electron (which is the case for all of the species studied in this work), and the LUMO corresponds to an appropriate antibonding orbital (C=S π^* for RAFT species and N—C σ^* for NMP) that could conceivably be involved in resonance (or hyperconjugative) stabilization of the unpaired electron. This latter property is satisfied for all of the present species except TMIO, for which the LUMO corresponds to the π^* orbital of the phenyl ring, a group that is not conjugated with the unpaired electron. As a result, the HOMO—LUMO gap gives rise to a resonance descriptor for TMIO that is unreasonably large. In this case we use the higher-energy orbital LUMO+3 in place of the LUMO to give the corresponding N—C σ^* antibonding orbital (see Figure S1 of the Supporting Information). For all atomic species (in this case all of the halogens in ATRP) we set the resonance descriptors to zero because atoms do not have adjacent functional groups with which they can undergo resonance or hyperconjugation. Full details of all parameters and their associated values are provided in Table 5; Figure 3 shows their values for the X-groups in the current work, converted to dimensionless units for ease of comparison.

From Figure 3, it is seen that, taken collectively, the X-descriptors can be used to identify the general type of controlled radical polymerization (CRP) process. Specifically, the halogens (ATRP) are characterized by having zero values for resonance and small steric parameters and the largest polar parameters; the nitroxides (NMP) have the smallest polar parameters, large steric parameters and intermediate resonance parameters; the dithioesters (RAFT) are characterized by having consistently large values of all of the parameters. These broad trends in the X values mirror to some extent those of the corresponding R-group weightings from Table 6. Thus, for example, the polar X-descriptor is largest for halogens, and the weighting of the polar R-descriptor in eq 2 was largest when X was a halogen; likewise the steric X-term is largest for NMP and RAFT and the weighting of the steric R-term was also largest for these X-groups in eq 2. Clearly, steric R-group effects are likely to be much more significant if X is also sterically hindered; likewise, the significance of polar R-group effects (measured here as the electron donation capacity of R) will depend on the polarity of X (measured here as its electron accepting capacity). In this way, some of the

interaction between R and X can be modeled from information on the isolated properties of R and X.

The resonance R- and X- descriptors behave more independently, as, unlike the steric and polar terms, their contributions to bond energies are more related to the stabilities of the R• and X• fragments rather than the R—X bond. It should also be pointed out that the resonance R-descriptor, the RSE of R•, depends not only on the resonance properties of R, but also includes contributions from induction and steric effects that cannot be completely separated. In contrast, the resonance X-descriptor, the inverse HOMO—LUMO gap of X•, is more directly related the resonance effect. Nonetheless, to a large extent, each of these descriptors focuses on those properties of R and X that affect the stabilities of isolated R• and X•, rather than the R—X bond. As a result, the resonance X-parameters help to model some of the major systematic differences between R—X BDFEs as X is varied both between series and within series, though the other X-descriptors (particularly the polar term) also makes significant contributions. Thus, the strongest bonds (i.e., X = halogen) have the smallest resonance parameters, while the weaker bonds (i.e., X = nitroxide, dithioester) have much larger resonance parameters. However, although the resonance parameter is generally largest for the dithioesters, their bonds are stronger on average than for the nitroxides due to their additional strengthening by polar effects.

Within each individual series of halogens, nitroxides and dithioesters there is also some variation in the values of the steric, polar and resonance parameters, which helps to model their differing contributions to the R—X bond energies. The steric parameter decreases slightly from Cl > Br > I reflecting the increasingly longer R—X bond length in these cases. The steric parameter in the dithioesters remains largely constant, reflecting the limited impact of the remote Z-group on the steric bulk of S=C(Z)S• functional group. The steric parameter in the nitroxides varies slightly in accord with the crowding about the nitrogen with the acylic DBN having the largest parameter and the planar TMIO radical having the smallest. The polar terms show more variation with the halogens decreasing from Cl > Br > I in accord with the expected decrease in electronegativity as the valence electrons are increasingly shielded from the nucleus. The variation in the EA of the dithioesters reflects the lone pair donor/σ acceptor properties of the Z-group, with the strong σ acceptor fluorine giving rise to the largest EA and the strong lone pair donor NEt$_2$ giving rise to the smallest. As we have found in our previous studies of the redox chemistry of nitroxides,[16] the EA values of the nitroxides are largely governed by the flexibility of the nitrogen to pyramidalize upon forming the anion with steric hindrance toward to pyramidalization being least in TEMPO, larger in DBN due to the nonbonded interactions in the *t*-butyl groups and larger still in the five-membered PROXYL. An exception to this trend is TMIO, which has a fused five-membered ring that resists planarization. On this basis, it should have had the most negative EA but is actually the most easily reduced. The reason for this is that, unlike the other species, it contains an aromatic ring which, though not conjugated with the NO functional group, nonetheless helps to stabilize the negative ion by accepting electrons. Indeed calculated charge distributions show that, in contrast to the other nitroxides, the NO functionality in TMIO is almost neutral in the anion (see Figure S2 of the Supporting Information). It should be stressed, however, that the aromatic ring does not delocalize the unpaired electron of the radical and its orbital diagram is almost identical to that of

Table 7. Coefficients and Associated Statistical Testing for Fitting of Equation 5: BDFE $[R-X] = a\,\theta[R] + b\,IP[R] + c\,RSE[R] + d\,\theta[X] + e\,EA[X] + f\,Resonance[X] + g$ to the Various Sets of Solution-Phase R−X BDFEs in which R and X Vary Simultaneously [a]

	training set	everything	ATRP only	RAFT only	NMP only
% contribution $\theta[R]$	2	2	4	2	13
% contribution IP[R]	4	3	14	2	21
% contribution RSE[R]	10	9	34	7	66
% contribution $\theta[X]$	29	29	36	89	—
% contribution EA[X]	34	34	12	—	—
% contribution resonance[X]	21	23	—	—	—
a	−21.9	−20.8	−13.8	−25.0	−28.3
b	−10.5	−9.73	−11.3	−6.43	−10.9
c	−1.04	−1.10	−1.04	−0.93	−1.39
d	214	192	240	−356	—
e	64.9	57.4	51.2	—	—
f	−63.2	−62.0	—	—	—
g	−324	−250	−356	1499	339
R^2 on fitted data	0.99	0.96	0.96	0.88	0.92
R^2 on training set	0.99	0.98	—	—	—
R^2 on test set I	0.96	0.97	—	—	—
R^2 on test set II	0.89	0.89	—	—	—
R^2 on everything	0.96	0.96	—	—	—
MAD on fitted data	5.6	9.6	6.7	5.5	8.9
MAD on training set	5.6	7.8	—	—	—
MAD on test set I	9.1	8.7	—	—	—
MAD on test set II	17.9	13.9	—	—	—
MAD on everything	10.0	9.6	—	—	—

[a] Parameters obtained by fitting each equation to each relevant data set, as noted in the table: the "training set" is defined in Scheme 2 and Table 1; "everything" is all available data (i.e., as listed in Tables 1−3); "ATRP" is the subset of "Everything" where X is a halogen; "RAFT" is the subset of "Everything" where X is a dithioester fragment; "NMP" is the subset of "Everything" where X is a nitroxide. For the individual fits, some of the parameters were found to be not statistically significant at a 95% level of confidence so they were removed and the equations were then refitted. For each fitted equation, % contributions were calculated via eqs 3 and 4. The ability of the equation to describe/predict BDFE data was quantified through the R^2 value and mean absolute deviation of predicted from actual BDFEs (MAD, kJ mol^{-1}), evaluated for the data to which the equation was fitted ("fitted data"), all available data ("everything") and the various training and test sets, as defined in Scheme 2.

PROXYL (see Figure S1 in the Supporting Information). Despite these small differences, the major observation is that none of these nitroxides are very easily reduced in the gas phase—their vertical EA values are either weakly negative or close to zero, and their adiabatic values (not shown) are only very weakly positive—and this is why their polar effects are minimal. With exception of the halogens, for which the resonance parameters are all zero, the resonance X$^\bullet$ parameters also show variation within a series. For the dithioesters, the resonance parameter is governed by the ability of the conjugated X group to stabilize the thiyl radical with Z-groups such as phenyl giving rise to larger values than aliphatic groups or lone pair donors. The resonance parameters for the nitroxides are relatively constant reflecting the fact that none of these species are conjugated with remote functional groups (as in the dithioesters), and their local environment is the same at the α, β, and γ positions.

Simultaneous Variation of R and X. Using these three X-descriptors, and the corresponding steric (θ), polar (IP), and radical stability (RSE) R-descriptors from the previous section, we constructed the following linear free energy relationship.

$$BDFE[R-X] = a\theta[R] + bIP[R] + cRSE[R] + d\theta[X] + eEA[X] + f\,Resonance[X] + g \quad (5)$$

As in the previous equations, the prefactors are optimized for values of the descriptors in their units of Tables 4 and 5 (that is,

eV for IP and EA, hartree^{-1} for resonance, kJ mol^{-1} for RSE, and radian for θ). The model was first fitted to the training set, so that we could test its ability to reproduce not only the data to which it was fitted, but also its predictive power across the test sets. Table 7 shows the resulting values of the fitted parameters ($a-g$) along with the % contributions of each term (as calculated using eqs 3 and 4), and the relevant R^2 and MAD values. We then refitted the equation to all available data, and also to subsets of the complete data set in which X was either a halogen of any type (labeled "ATRP" in Table 7), dithioester of any type ("RAFT") or nitroxide of any type ("NMP"). These results are also included in Table 7. To illustrate the predictive power of the various fitted equations, Figure 4 shows the predicted versus actual BDFEs according to whether the equation is fitted only to the training set or whether it is refitted to all available data. Figure 5 shows the predicted versus actual BDFEs when one uses 3 separate equations for ATRP, NMP, and RAFT.

From Table 7, we first note that our model provides an excellent fit to the training set (MAD = 5.6 kJ mol^{-1}), and does a very reasonable job of predicting the BDFEs in test set I (MAD = 9.1 kJ mol^{-1}). However, its performance for test set II is much poorer (MAD = 17.9 kJ mol^{-1}). If one refers back to Scheme 2, it is seen that the training set contains 21 different R-groups but only 4 X-groups to represent all ATRP, RAFT, and NMP processes. It is therefore not surprising that the equation
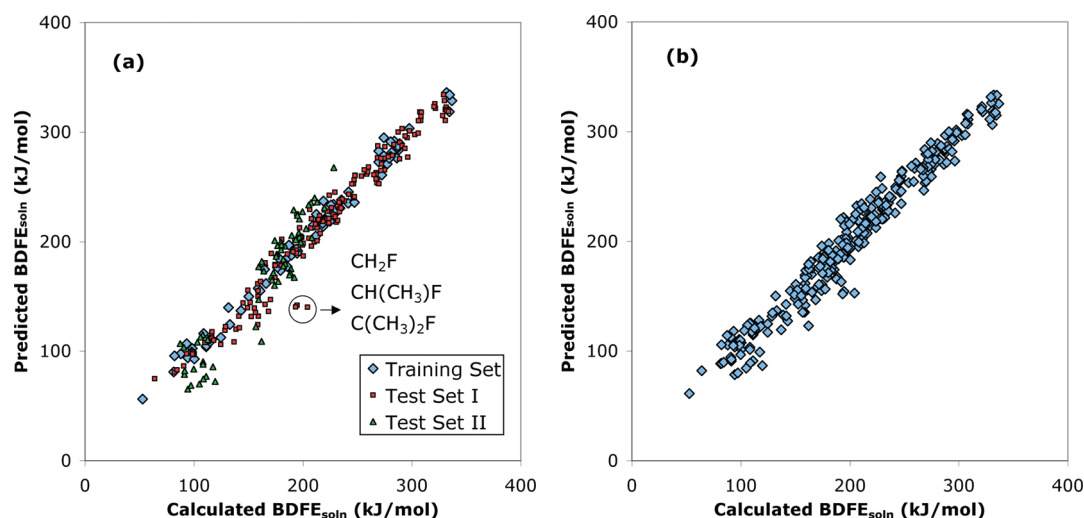
Figure 4. Predicted vs calculated BDFEs for simultaneous fits of eq 5 to ATRP, NMP, and RAFT when (a) fitted to training set and then tested on test set I and test set II and (b) refitted to all available data.
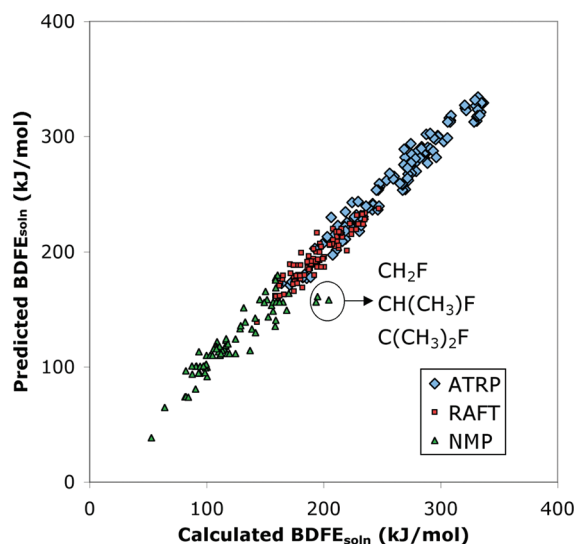

Figure 5. Predicted vs calculated BDFEs for fits of eq 5 using separate equations for ATRP, RAFT, and NMP, respectively.

performs well for test set I, which expands the range of R-groups, but poorer for Test Set II, which expands the range of X-groups. When the equation is refitted to all of the available data, the performance of the model for test set II improves considerably though it still remains poor compared with the R-dominated data sets, i.e., training set or test set I (MAD = 13.9 versus 7.8 or 8.7 kJ mol^{-1}). The worst outliers occur for the various fluorine substituted R-groups in NMP, and are due to anomeric strengthening of the breaking bond that is not captured in the model.[5] Nonetheless, the overall performance of eq 5 against the complete data set is relatively good both for the equation fitted only the Training Set and the equation refitted to all available data (MAD = 10.0 and 9.6 kJ mol^{-1} respectively). This MAD is approximately twice the typical uncertainty in theoretical or experimental BDFEs, and translates into an uncertainty of approximately 2 orders of magnitude in the resulting equilibrium constant at room temperature. Although this may seem large, it

needs to be remembered that the BDFEs in Tables 1−3 vary over a range of 284 kJ mol^{-1}, and hence the error is effectively only 4%. The model would thus be of practical value in the first stage of a reagent design process, allowing one to narrow a large field to a smaller number of candidates that could then be subjected to more precise experimental and/or quantum-chemical evaluation.

It is clear that modeling the effect of X on the BDFEs as X is changed from halogens to nitroxides to dithioester fragments poses the greatest challenge to developing a general linear free energy relationship for these processes; by comparison, modeling the effect of the alkyl fragment on the BDFEs is relatively straightforward. This is further reinforced when we examine the results for equations that are separately fitted to ATRP, RAFT, or NMP data. It should be stressed that these data sets also allow simultaneous variation of R and X; however, variation of X is restricted to within a set of halogens (ATRP), dithioester fragments (RAFT), or nitroxide radicals (NMP). In those cases the MADs are much smaller, particularly for ATRP and RAFT (6.7 and 5.4 kJ mol^{-1} respectively). These individually fitted equations should thus be preferred when modeling the variation of R and X within a class of polymerization.

For NMP, the MAD for the individual fit (8.6 kJ mol^{-1}) does not improve as much as in RAFT and ATRP. This is in part because the data sets include alkyl radicals with an α lone pair donor groups capable of imparting extra stabilization to the O−R bond of the alkoxyamine. As explained above, these anomeric effects are not taken into account in the model,[5] and are responsible for the worst of these outliers in Figures 4 and 5. In addition, none of the X-descriptors are statistically significant when the equation is fitted to the NMP subset, implying that they are less suitable for modeling the substituent effects on this process. Indeed, our previously published equation for NMP uses a different (single) X-descriptor, RSE$_{nxd}$, and performs much better (MAD 4.5 kJ mol^{-1}).[5] This equation would be preferred if one was studying NMP alone. This highlights another compromise that is required when modeling the simultaneous variation of R and X across different types of polymerization process from knowledge of the separate properties of R and X. Not only do the relative importance of steric, polar and radical stability or resonance effects change, but also the suitability of the

descriptors for modeling these properties. These problems place fundamental limits on the predictive power of linear free energy relationships. Nonetheless, in the context of the wide variation of BDFEs in Tables 1−3, all of the equations in Table 7 do a very reasonable job of predicting R—X BDFEs on the basis of the isolated properties of R and X.

Analysis of Parameter Contributions. Given the differences in structure—reactivity trends between ATRP, NMP and RAFT, it is remarkable that the general model performs as well as it does. It is thus worth examining how the weightings of the various descriptors in the general equation change from their "optimum" values in individual equations for NMP, ATRP, and RAFT so as to correct for the differing roles of polar, steric and resonance effects in the various processes, and to model the large quantitative differences between average R—X BDFEs for the different classes of X.
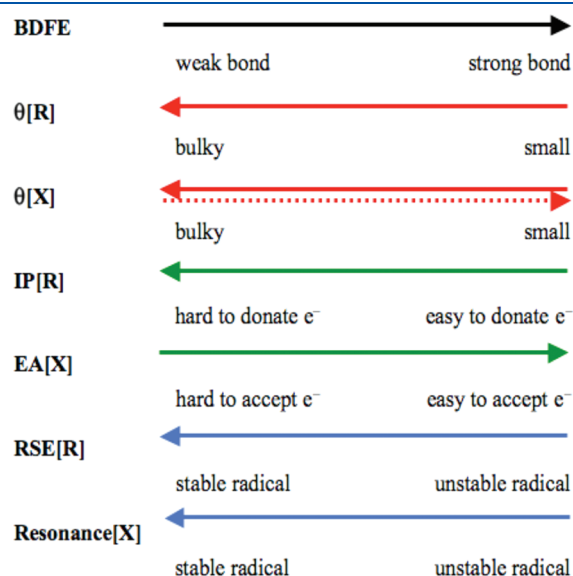

Figure 6. Contributions of the descriptors to bond strength. Arrows point in the direction of increasing descriptor values, and if they are the same direction as BDFE, the sign in eq 5 is positive, and vice versa. The dash arrow indicates that the sign of $\theta[X]$ has reversed when the eq 5 is fitted the combined data or the ATRP data. See text for more detail.

If we first examine the coefficients and the %contributions of the alkyl group polar, steric and radical stability terms in the various fitted equations (Table 7), it is clear that the contributions of these R-descriptors remain *qualitatively* independent of the data set to which the equation was fitted, and make physical sense. Thus, the fitted coefficient of $\theta[R]$ is always negative, implying that the BDFE decreases (i.e., the bond becomes more easily broken) as the R-group becomes more bulky. The fitted coefficient of IP[R] is also always negative implying that the BDFE decreases (i.e., bond is more easily broken) as the R-groups become less easily oxidized and hence less stable as cations. This is consistent with the notion that the R—X bonds in these systems may be stabilized by resonating between their covalent (R—X) and ionic forms (R$^+$X$^-$), the latter becoming more significant as R becomes a better donor and hence more stable as a cation. The fitted coefficient of the RSE is also always negative implying that the BDFE decreases as R$^\bullet$ becomes more stable as a radical, since this implies stabilization of the products of the bond homolysis relative to the bond itself. These trends are summarized in Figure 6, where it is seen that a high BDFE corresponds to R and X groups that are nonsterically hindered, respectively good donors and acceptors, and not very stable as isolated radicals.

While the role of R-descriptors is qualitatively independent of the fitting set, there are some quantitative differences. To illustrate these, Figure 7 shows the %contributions of each of the R-descriptors as obtained by fitting the equation to all available data or to the ATRP, NMP or RAFT subsets. For ease of comparison we plot the "raw" contributions and also the corresponding relative values (as obtained by normalizing them to the same total contribution for the three R-descriptors). Consistent with our studies where X was fixed, it is again clear that the relative contributions of the steric, polar and resonance descriptors do change according to the nature of X, whereas in Figure 7b, the resonance/radical stability contribution is similar across all three types of process, the steric contribution is significantly lower, and the polar contribution is significantly higher in ATRP compared with NMP and RAFT. The total % contribution of the R descriptors (versus the X-descriptors) in Figure 7a also varies with the nature of X and this balance is a compromise in the general equation.

In the case of the X-descriptors the signs as well as the magnitudes of the coefficients change if the equation is refitted
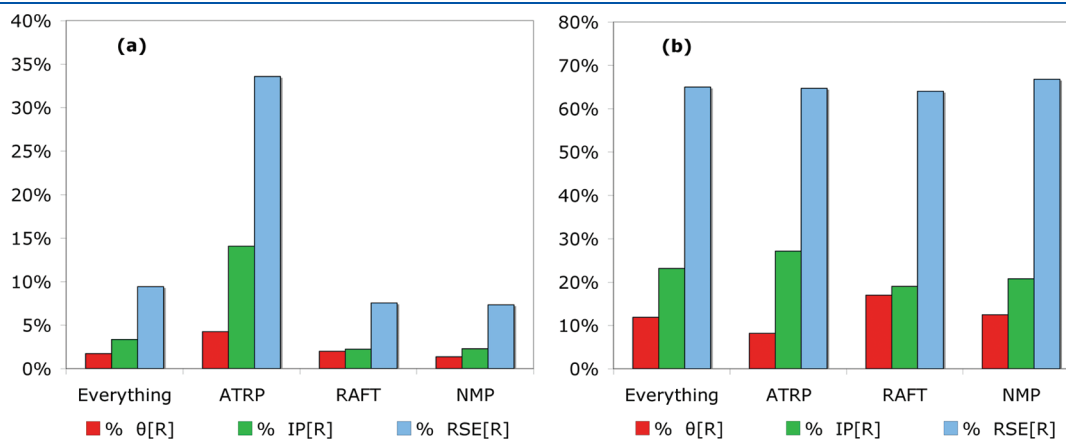

Figure 7. % Contribution of the steric, polar and radical stability R-descriptors to the eq 5 as fitted to all available data ("Everything"), or to subsets where X is restricted to either a halogen ("ATRP"), dithioester fragment ("RAFT") or nitroxide ("NMP"). Plot a shows the actual % contributions, while plot b shows the same data normalized to the same total % contribution of the R-descriptors.

to a subset of the total data in which only one type of polymerization process is represented. Indeed, when this is done, some of the X-descriptors become statistically redundant, with ATRP requiring only the polar and resonance descriptors, RAFT requiring only the steric descriptor and NMP requiring none of these X-descriptors. This "redundancy" in describing the properties of X is used in the full equation to take account of the major differences in R—X BDFEs when X is changed from a halogen to a nitroxide to a dithioester. As a result, some of the X-descriptors appear (at least in part) to take on qualitatively different roles in the general equation compared with the individual equations for ATRP, NMP, or RAFT.

For the polar and resonance terms, the signs of the prefactors are preserved across all data sets where they are significant and make physical sense. Thus, as shown in Figure 6, the BDFE is decreased by an increase in the resonance stabilization of X$^{\bullet}$, and increases with increasing EA (i.e., as X$^{\bullet}$ becomes a better electron acceptor) due to the increasing polar stabilization of the R—X bond. The steric term also makes physical sense in the RAFT equation, where the negative sign is implying a decrease in BDFE as the X-group becomes more bulky. However, for the ATRP equation and the general equation, the sign of the steric parameter reverses. In the case of the ATRP equation, this is because the steric term takes on the job of accounting for the major systematic differences in covalent bond strength due to factors such as orbital overlap when the halogen is changed from Cl to Br to I. Within the individual NMP or RAFT series these differences are minimal as the same type of covalent bond is being broken each time (i.e., C—O for NMP and C—S for RAFT), and so this effect can be built into the intercept term. For the ATRP subset, however, the nature of the bonded atoms changes as X is varied, and with that their covalent bond strength. In fact, orbital overlap in R—X (and hence covalent bond strength) decreases as the halogen is varied down the periodic table. Because the steric term also decreases in this direction (as a result of the lengthening bond), and because the actual steric effects in the halides are small, the steric term is used to model these differences and takes on a positive sign. This role reversal for the steric descriptor also occurs in the equations fitted simultaneously to the different types of polymerization process, and succeeds in part because the steric differences within a series of dithioesters or nitroxides, and indeed between the nitroxides and dithioesters are relatively small (see Figure 3). However, because the steric terms for the halogens are significantly smaller than for the dithioesters or nitroxides, the sign reversal and amplified importance for the steric term would lead to an underestimation of the BDFEs for the halides, versus the nitroxides and dithioesters. To compensate, the importance of the resonance and polar X-descriptors, which are indeed responsible for the stronger bonds of halides versus nitroxides or dithioesters, becomes enhanced.

To summarize this section, the linear free energy relationship succeeds in modeling the R—X BDFE across these three very classes of compounds, using the X-parameters (which, when taken together as a set, are very distinctive of the class of compound being studied) to model the large average differences between BDFEs as X is changed. The success is also due to the fact that, although there are some quantitative differences in the relative importance of polar and steric R-group effects when X is changed, these are relatively small and it is possible to capture them in a single fitted model. It is this neglected interaction between R and X that gives rise to the average error in the model of ±10 kJ mol^{-1}, when tested on the entire data set. As shown

earlier, this error can of course be reduced significantly (to the order of ±5 kJ mol^{-1}) simply by reparameterizing this model to data for the individual ATRP, NMP, or RAFT processes, and these reparameterized equations would be recommended when studying the processes in isolation.

Practical Aspects. With our equation in hand, we are now in a position to use it to identify suitable leaving groups and block-order sequences for controlled radical polymerization processes. In this regard, it is important to stress that in choosing suitable control agents there are two key aspects that need to be optimized. The first is the kinetics of the exchange between the dormant and active species; the second is the efficiency with which the leaving group on the initial control agent (which in the case of a block copolymer synthesis would be the first block of the copolymer) is displaced by the new propagating radical. To optimize the exchange rate, one needs to reparameterize the equations for the kinetics of the specific individual exchange reactions. As we have shown previously[5] for NMP this reparameterization should be possible, but is beyond the scope of the present work. However, the current equations can instead be used to optimize the leaving group efficiency, as this depends largely on the equilibrium position of the overall chain transfer reaction.[27] As shown earlier in Scheme 1, this chain transfer energy is simply the difference of the two relevant BDFEs, each of which can be predicted using eq 5 in conjunction with the relevant values of the R- and X-descriptors in Tables 4 and 5. In other words, the equations can be used to help choose suitable R-groups for the initial RAFT agents, alkyl halides, or alkoxyamines, and to help determine the correct sequence of monomer additions in block copolymer synthesis.[27]

To illustrate how this might work in practice, we use eq 5 to test whether or not some given leaving group (we have chosen the AN unimer radical for this example) is likely to be displaced from the initial alkyl halide, RAFT agent or alkoxyamine by various common propagating radicals. To this end, we use eq 5 to calculate the overall Gibbs free energy change for the following chain transfer reaction as the difference of the predicted AN—X and R—X BDFEs; for a suitable R-group, the reaction should be exoergic.[27]

$$R^{\bullet} + AN-X \rightarrow R-X + AN^{\bullet} \qquad (6)$$

In this example, we consider cases where X is either Cl, Br, I, SC(CH$_3$)=S, SC(OCH$_3$)=S, SC(SCH$_3$)=S, SC(NEt$_2$)=S, SC(Ph)=S, TEMPO, PROXYL, DBN, or TMIO, and R is a unimeric propagating radical of VA, MA, or MMA (see Scheme 2 for chemical structures). We note that some of these R and X combinations are unsuitable for controlled radical polymerization on the basis of poor exchange rates or side reactions; we include all of them here to provide a more consistent and broadly based test of the ability of eq 5 to predict chain transfer energies. Figure 8a shows the actual chain transfer energies as a function of R and X (as calculated directly from their ab initio BDFEs in Tables 1—3); Figure 8b shows the corresponding predictions of eq 5 made using the R-descriptors of Table 4.

Before examining the results, it should be noted that whereas the actual chain transfer energies depend on both R and X, the predictions of eq 5 are independent of X. This is because, as in any linear free energy relationship, the overall R—X BDFE is represented as a function of the *separate* contributions of the R and X components and, since X is common to AN—X and R—X, the X-contribution cancels. This is not to say that the X-components have no influence on the results—they do affect the
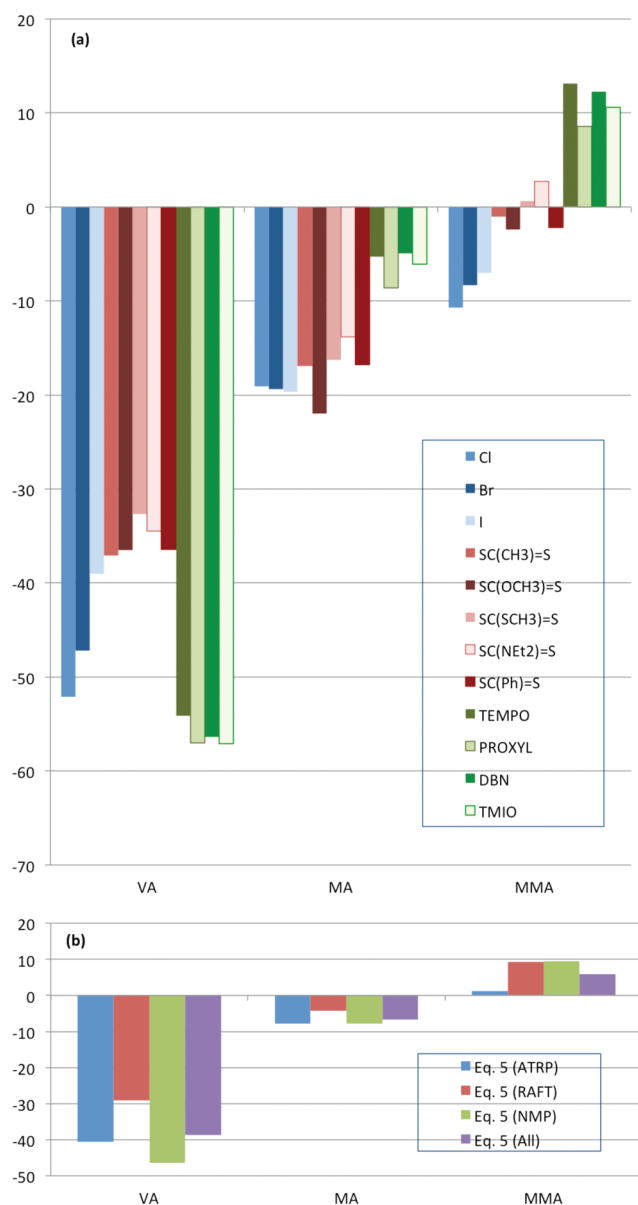
Figure 8. Chain transfer free energies (kJ mol^{-1}, acetonitrile, 298.15 K) for AN$-$X + R$^{\bullet}$ $\rightarrow$ AN$^{\bullet}$ + R$-$X where R = VA, MA and MMA (i.e., unimeric propagating radicals) and various X groups as shown. Chart a shows the directly calculated values for the various X groups. Chart b shows the corresponding predictions of eq 5, using versions of this equation fitted individually to ATRP, RAFT, or NMP, and also to the complete data set (All).

weighting of the various R-descriptors in the parametrized equation. The problem is that these weightings by necessity reflect the average influence of X over the whole training set and any single equation is unable to discriminate between the subtle variations in the weightings of polar, steric and resonance properties that occur as the X-group is changed. As explained earlier, this fundamental limitation is why the predictions of the equation are associated with a mean absolute deviation of approximately ±10 kJ mol^{-1}—deviations of this level or less are due to the *interactions* between R and X which can only be fully quantified by calculating or measuring the specific R$-$X BDFE directly (rather than predicting it in advance). However,

these problems are reduced if we use multiple versions of eq 5 that have each been fitted to separate data sets of alkyl halides (ATRP), dithioesters (RAFT) and alkoxyamines (NMP); these predictions are also included in Figure 8b. By narrowing the training set, one improves the accuracy of the model at the expense of some of its scope.

From Figure 8, we first note that the directly calculated reaction energies indicate that the chain transfer reaction is strongly exoergic for VA, moderately exoergic for MA, and varies between exoergic and endoergic for MMA, according to the nature of X. Specifically, for MMA, the chain transfer reaction is exoergic for the halogens (ATRP), varies between exoergic and endoergic for the dithioesters (RAFT), and is endoergic for the nitroxides (NMP). On this basis, one can infer that the AN leaving group would successfully be displaced by the unimeric propagating radical in VA and MA polymerization but for MMA polymerization it would be displaced only for the halides and certain RAFT agents. To the extent that these unimeric propagating radicals model their corresponding polymeric counterparts, one would also predict that AN should be the first block in block copolymer synthesis with VA or with MA, but with MMA it would depend upon the nature of the control agent. This is also consistent with practical experimental observations; for instance, AN is known to be a good initiating group for MMA polymerization in ATRP,[28] but not in RAFT.[3,29] Likewise, acrylate$-$acrylonitrile block copolymer synthesis via either ATRP or NMP is most efficient when the acrylonitrile block is polymerized first; though the order may be reversed for ATRP using a halogen exchange technique.[30]

If we compare the actual chain transfer energies in Figure 8 with the predictions of eq 5, we note that these are broadly consistent. The globally fitted version of eq 5 correctly predicts that the reaction is strongly exoergic for VA and moderately exoergic for MA, and hence that AN would be successfully displaced by the propagating radical for these two polymerizations. For MMA polymerization, eq 5 predicts that the reaction is weakly endoergic and hence not capable of displacing the MMA propagating radical—which is the correct result for some but not all of the X-groups. Importantly, the magnitude of the predicted endothermicity is within ±10 kJ mol^{-1} of zero, and hence the Eq5 predictions are sufficiently close to zero to prompt further scrutiny. These broad predictions are further improved by using the separate versions of eq 5 for ATRP, RAFT, and NMP, which do a good job of capturing the main qualitative differences between the different types of process, including the greatly reduced exoergicity for the chain transfer reactions of the MMA radicals with alkyl halides, compared with alkoxyamines or dithioesters.

Of course the predictions are still not perfect. In particular, eq 5 still slightly overestimates the chain transfer energy with MMA for the halides and with some of the RAFT agents. The former result was discussed earlier in the context of eq 2 and stems from the differing impact of π and σ effects on the value of the polar descriptor versus the bond strength for this particular functional group; the latter result is because the model fails to account for the anomeric weakening of the AN$-$RAFT bond[31] for certain RAFT agents. The presence or absence of this anomeric effect causes the considerable variation in the chain transfer energy as the Z-group of the RAFT agent is changed; the X-independent eq 5 predictions are closer to the most endothermic values, which occur when these effects are absent. In a similar manner, the equation underestimates the exothermicity

of the chain transfer reactions with VA in NMP by failing to account for the anomeric strengthening of the formed C—O bond. These variable specific interactions are clearly beyond the scope of any general linear free energy relationship (or qualitative structure—reactivity study) that seeks to predict the behavior of any new R and X combination based on the knowledge of R and X separately. These limitations need to be recognized, and the predictions need to be considered in the context of the residual error in the model (ca. $\pm$ 10 kJ mol^{-1} for the general eq 5 and the NMP version; $\pm$ 5 kJ mol^{-1} for the RAFT and ATRP versions). Nonetheless, as this example shows, eq 5 is capable of ruling out unsuitable block orders and initiators, as a first pass at optimizing the leaving group on the control agent. Moreover, the individual ATRP, RAFT and NMP equations do an excellent job of capturing some broad differences between ATRP, NMP, and RAFT and providing a deeper understanding of the stereoelectronic properties that lead to these similarities and differences.

CONCLUSIONS

High-level *ab initio* molecular orbital theory has been used to determine bond dissociation free energies of the dormant species for a wide range of ATRP, RAFT, and NMP systems, and correlate them with various polar, steric and radical stabilization descriptors for the control agent and alkyl radical. The multiparameter analysis is subsequently used to evaluate contribution of these factors to the equilibrium constants and to derive a general equation that predicts the equilibrium constant for other systems. The final equation is BDFE[R—X] = -20.8 θ[R] $-$ 9.73 IP[R] $-$ 1.10 RSE[R] $+$ 192 θ[X] $+$ 57.4 EA[X] $-$ 62.0 Resonance[X] $-$ 250, where the steric descriptors θ[R] and θ[X] are measured as Tolman's cone angle of Cl—R and CH$_3$—X respectively, the polar descriptors IP[R] and EA[X] are the (gasphase) ionization energy of R$^\bullet$ and electron affinity of X$^\bullet$ respectively, and the radical stability or resonance descriptors RSE[R] and Resonance[X] are measured as the standard radical stabilization energy for R$^\bullet$ and the inverse HOMO—LUMO energy gap for X$^\bullet$. This general model was able to predict the R—X BDFEs for any combination of R and X, based on the isolated properties of R and X alone, to within an average error of $\pm$10 kJ mol^{-1} or 4% of the total variation in the BDFEs. The model would thus be of practical value in the first stage of a reagent design process, allowing one to narrow a large field to a smaller number of candidates that could then be subjected to more precise experimental and/or quantum-chemical evaluation. Improved predictive power is possible (with errors of the order of $\pm$5 kJ mol^{-1}) when the model is refitted to BDFE data for a specific class of compounds (i.e., X = halides, or X = nitroxides, or X = dithioesters), and these reparameterized models would be favored for making refined predictions for a particular type of radical polymerization process. We are now using the descriptors developed during this study to tackle the more difficult problem of modeling the exchange rates in the individual controlled radical polymerization processes.

ASSOCIATED CONTENT

ⓢ Supporting Information.   Further computational details including molecular orbitals, charge distributions, complete optimized geometries of all species, all corresponding gas-phase bond energies. This information is provided free of charge via the Internet at http://pubs.acs.org

AUTHOR INFORMATION

Corresponding Author
*E-mail: mcoote@rsc.anu.edu.au.

ACKNOWLEDGMENT

REFERENCES

(1) For reviews, see for example:(a) Hawker, C. J.; Bosman, A. W.; Harth, E. *Chem. Rev.* **2001**, *101*, 3661. (b) Bertin, D.; Gigmes, D.; Marque, S. R. A.; Tordo, P. *Chem. Soc. Rev.* **2011**, *40*, 2189.

(2) For reviews, see for example:(a) Matyjaszewski, K. *Chem.—Eur. J.* **1999**, *5*, 3095–3102. (b) Matyjaszewski, K.; Xia, J. *Chem. Rev.* **2001**, *101*, 2921. (e) Braunecker, W. A.; Matyjaszewski, K. *Prog. Polym. Sci.* **2007**, *32*, 93. (c) Tsarevsky, N. V.; Matyjaszewski, K. *Chem. Rev.* **2007**, *107*, 2270–2299. (d) Matyjaszewski, K.; Tsarevsky, N. V. *Nature Chem.* **2009**, *1*, 276–288.

(3) (a) For reviews, see for example:Moad, G.; Rizzardo, E.; Thang, S. H. *Aust. J. Chem.* **2005**, *58*, 379. (b) Moad, G.; Rizzardo, E.; Thang, S. H. *Aust. J. Chem.* **2006**, *59*, 669. (c) Moad, G.; Rizzardo, E.; Thang, S. H. *Aust. J. Chem.* **2009**, *62*, 1402.

(4) See for example:(a) Fischer, H.; Marque, S. R. A.; Nesvadba, P. *Helv. Chim. Acta* **2006**, *89*, 2230. (b) Bertin, D.; Gigmes, D.; Marque, S. R. A.; Tordo, P. *Macromolecules* **2005**, *38*, 2638. (c) Marque, S. R. A. *J. Org. Chem.* **2003**, *68*, 7582.

(5) Hodgson, J. L.; Lin, C. Y.; Coote, M. L.; Marque, S. R. A.; Matyjaszewski, K. *Macromolecules* **2010**, *43*, 3728.

(6) See, for example:(a) Seeliger, F.; Matyjaszewski, K. *Macromolecules* **2009**, *42*, 6050–6055. (b) Pintauer, T.; Matyjaszewski, K. *Chem. Soc. Rev.* **2008**, *37*, 1087–1097. (c) Tang, W.; Kwak, Y.; Braunecker, W.; Tsarevsky, N. V.; Coote, M. L.; Matyjaszewski, K. *J. Am. Chem. Soc.* **2008**, *130*, 10702. (d) Tang, W.; Matyjaszewski, K. *Chem. Rev.* **2007**, *40*, 1858. (e) Tang, W.; Matyjaszewski, K. *Macromolecules* **2006**, *39*, 4953. (f) Pintauer, T.; Matyjaszewski, K. *Coord. Chem. Rev.* **2005**, *249*, 1155–1184.

(7) See for example:(a) Coote, M. L.; Krenske, E. H.; Izgorodina, E. I. *Macromol. Rapid Commun.* **2006**, *27*, 473. (b) Chiefari, J.; Mayadunne, R. T. A.; Moad, C. L.; Moad, G.; Rizzardo, E.; Postma, A.; Skidmore, M. A.; Thang, S. H. *Macromolecules* **2003**, *36*, 2273–2283. (c) Chong, Y. K.; Krstina, J.; Le, T. P. T.; Moad, G.; Postma, A.; Rizzardo, E.; Thang, S. H. *Macromolecules* **2003**, *36*, 2256–2272.

(8) (a) Alfrey, T.; Price, C. C. *J. Polym. Sci.* **1947**, *2*, 101. (b) Price, C. C. *J. Polym. Sci.* **1948**, *3*, 752.

(9) Guillaneuf, Y.; Gigmes, D.; Marque, S. R. A.; Astolfi, P.; Greci, L.; Tordo, P.; Bertin, D. *Macromolecules* **2007**, *40*, 3108.

(10) Frisch, M. J.; Trucks, G. W.; Schlegel, H. B.; Scuseria, G. E.; Robb, M. A.; Cheeseman, J. R.; Montgomery, J. A., Jr.; Vreven, T.; Kudin, K. N.; Burant, J. C.; Millam, J. M.; Iyengar, S. S.; Tomasi, J.; Barone, V.; Mennucci, B.; Cossi, M.; Scalmani, G.; Rega, N.; Petersson, G. A.; Nakatsuji, H.; Hada, M.; Ehara, M.; Toyota, K.; Fukuda, R.; Hasegawa, J.; Ishida, M.; Nakajima, T.; Honda, Y.; Kitao, O.; Nakai, H.; Klene, M.; Li, X.; Knox, J. E.; Hratchian, H. P.; Cross, J. B.; Adamo, C.; Jaramillo, J.; Gomperts, R.; Stratmann, R. E.; Yazyev, O.; Austin, A. J.; Cammi, R.; Pomelli, C.; Ochterski, J. W.; Ayala, P. Y.; Morokuma, K.; Voth, G. A.; Salvador, P.; Dannenberg, J. J.; Zakrzewski, V. G.; Dapprich, S.; Daniels, A. D.; Strain, M. C.; Farkas, O.; Malick, D. K.; Rabuck, A. D.; Raghavachari, K.; Foresman, J. B.; Ortiz, J. V.; Cui, Q.; Baboul, A. G.; Clifford, S.; Cioslowski, J.; Stefanov, B. B.; Liu, G.; Liashenko, A.; Piskorz, P.; Komaromi, I.; Martin, R. L.; Fox, D. J.; Keith, T.; Al-Laham, M. A.; Peng, C. Y.; Nanayakkara, A.; Challacombe, M.; Gill, P. M. W.; Johnson, B.; Chen, W.; Wong, M. W.; Gonzalez, C.; Pople, J. A., *Gaussian 03, Revision B.03*; Gaussian, Inc.: Pittsburgh PA, 2003.

(11) MOLPRO, version 2009.1, a package of ab initio programs written by Werner, H.-J.; Knowles, P. J.; Manby, F. R.; M. Schütz, Celani, P.; Knizia, G.; Korona, T.; Lindh, R.; Mitrushenkov, A.; Rauhut, G.; Adler, T. B.; Amos, R. D.; Bernhardsson, A.; Berning, A.; Cooper, D. L.; Deegan, M. J. O.; Dobbyn, A. J.; Eckert, F.; Goll, E.; Hampel, C.; Hesselmann, A.; Hetzer, G.; Hrenar, T.; Jansen, G.; C. Köppl, Liu, Y.; Lloyd, A. W.; Mata, R. A.; May, A. J.; McNicholas, S. J.; Meyer, W.; Mura, M. E.; Nicklaß, A.; Palmieri, P.; K. Pflüger, Pitzer, R.; Reiher, M.; Shiozaki, T.; ,Stoll, H.; Stone, A. J.; Tarroni, R.; Thorsteinsson, T.; Wang, M.; Wolf, A. ; see http://www.molpro.net.

(12) See, for example: Coote, M. L.; Lin, C. Y.; Beckwith, A. L. J.; Zavitsas, A. A. *Phys. Chem. Chem. Phys.* **2010**, *12*, 9597.

(13) See, for example: Lin, C. Y.; Coote, M. L.; Gennaro, A.; Matyjaszewski, K. *J. Am. Chem. Soc.* **2008**, *130*, 12762.

(14) See, for example: Hodgson, J. L.; Roskop, L. B.; Gordon, M. S.; Lin, C. Y.; Coote, M. L. *J. Phys. Chem. A* **2010**, *114*, 10458.

(15) See, for example:(a) Chernikova, E.; Golubev, V.; Filippov, A.; Lin, C. Y.; Coote, M. L. *Polym. Chem.* **2010**, *1*, 1437. (b) Lin, C. Y.; Coote, M. L. *Aust. J. Chem.* **2009**, *62*, 1479–1483.

(16) (a) Hodgson, J. L.; Namazian, M.; Bottle, S. E.; Coote, M. L. *J. Phys. Chem. A* **2007**, *111*, 13595–13605. (b) Blinco, J. P.; Hodgson, J. L.; Morrow, B. J.; Walker, J. R.; Will, G. D.; Coote, M. L.; Bottle, S. E. *J. Org. Chem.* **2008**, *73*, 6763–6771.

(17) Scott, A. P.; Radom, L. *J. Phys. Chem.* **1996**, *100*, 16502.

(18) Izgorodina, E. I.; Lin, C. Y.; Coote, M. L. *Phys. Chem. Chem. Phys.* **2007**, *9*, 2507.

(19) Henry, D. J.; Sullivan, M. B.; Radom, L. *J. Chem. Phys.* **2003**, *118*, 4849.

(20) See for example:(a) Izgorodina, E. I.; Coote, M. L. *J. Phys. Chem. A* **2006**, *110*, 2486. (b) Izgorodina, E. I.; Brittain, D. R. B.; Hodgson, J. L.; Krenske, E. H.; Lin, C. Y.; Namazian, M.; Coote, M. L. *J. Phys. Chem. A* **2007**, *111*, 10754. (c) Lin, C. Y.; Hodgson, J. L.; Namazian, M.; Coote, M. L. *J. Phys. Chem. A* **2009**, *113*, 3690.

(21) Rassolov, V. A.; Ratner, M. A.; Pople, J. A.; Redfern, P. C.; Curtiss, L. A. *J. Comput. Chem.* **2001**, *22*, 976.

(22) (a) Lin, C. Y.; Izgorodina, E. I.; Coote, M. L. *J. Phys. Chem. A* **2008**, *112*, 1956.(b) See: http://rsc.anu.edu.au/~cylin/scripts.html.

(23) (a) Klamt, A.; Schueuermann, G. *J. Chem. Soc., Perkin Trans. 2* **1993**, 799. (b) Cossi, M.; Rega, N.; Scalmani, G.; Barone, V. *J. Comput. Chem.* **2003**, *24*, 669.

(24) Shorter, J. *Correlation Analysis of Organic Reactivity*; J. Wiley & Sons: New York, 1982; pp 73−126.

(25) See for example:(a) Lin, C. Y.; Peh, J.; Coote, M. L. *J. Org. Chem.* **2011**, *76*, 1715–1726. (b) Shurki, A.; Hiberty, P. C.; Shaik, S. *J. Am. Chem. Soc.* **1999**, *121*, 822–834and references cited therein.

(26) For detailed analyses, see, for example:(a) Griller, D.; Ingold, K. *Acc. Chem. Res.* **1976**, *9*, 13–19. (b) Bernardi, F.; Epiotis, N. D.; Cherry, W.; Schlegel, H. B.; Whangbo, M.-H.; Wolfe, S. *J. Am. Chem. Soc.* **1976**, *98*, 469–478. (c) Zipse, H. *Top. Curr. Chem.* **2006**, *263*, 163–189. (d) Henry, D. J.; Parkinson, C. J.; Mayer, P. M.; Radom, L. *J. Phys. Chem. A* **2001**, *105*, 6750–6756.(e) Coote, M. L.; Lin, C. Y.; Zipse, H. In *Carbon-Centered Free Radicals: Structure, Dynamics and Reactivity*; Forbes, M. D. E., Ed.; Wiley: New York, 2010; pp 83−104. (f) Hioe, J.; Zipse, H. *Org. Biomol. Chem.* **2010**, *8*, 3609–3617. (g) Poutsma, M. L. *J. Org. Chem.* **2011**, *76*, 270–276.

(27) Of course, it is also essential that the leaving group reinitiate polymerization, which needs to be checked separately using either calculated or measured rate data or an equivalent linear free energy relationship for radical addition kinetics, as in: Fischer, H.; Radom, L. *Angew. Chem., Int. Ed.* **2001**, *40*, 1340. It is also essential that neither the leaving group, nor the propagating radical, undergo side reactions, which needs to be checked on a case-by-case basis. In essence, once can think of equation 5 as being used to rule out leaving groups that are incapable of being efficiently displaced from the initial control agent; however, the smaller number of remaining candidates then need to be checked for other unwanted properties.

(28) Magenau, A. J. D.; Kwak, Y.; Matyjaszewski, K. *Macromolecules* **2010**, *43*, 9682.

(29) In fact, when the same calculations are performed for dimer AN and MMA radicals, the penultimate unit effects make AN an unsuitable leaving group for all of the studied RAFT agents in MMA polymerization (consistent with experiment) though it remains viable for ATRP. Further work on penultimate unit effects is currently underway.

(30) Tang, C.; Kowalewski, T.; Matyjaszewski, K. *Macromolecules* **2003**, *36*, 1465–1473.

(31) Coote, M. L.; Henry, D. J. *Macromolecules* **2005**, *38*, 1415–1433.